Int. J. Electrochem. Sci., 16**(2021)** Article ID: 210928, doi: 10.20964/2021.09.39

International Journal of
ELECTROCHEMICAL
SCIENCE
www.electrochemsci.org

Electrochemical Photocatalytic degradation of Brilliant Blue FCF as food dye by CuO–TiO_2 nanocomposite under visible and UV-light irradiations

Yuqi Li

Department of Life Science, Lvliang University, Lvliang, 033000, China
E-mail: yuqili30@yahoo.com, liyuqi7868@163.com

Received: 24 May 2021/ *Accepted:* 5 July 2021 / *Published:* 10 August 2021

In this work, a simple deposition technique was used to synthesize CuO/TiO_2 nanocomposites and their application as photocatalysts for the photodegradation of Brilliant Blue FCF (BBF) under visible and UV-light irradiations were studied. The prepared nanocomposites and their components were investigated in terms of structural, morphological, electrochemical, optical, and photocatalytic degradation properties. When UV–Vis absorbance spectra were used to characterize photocatalysts, it was revealed that the bandgap reduced as the CuO concentration increased. TiO_2, CuO-TiO_2-0.5, CuO-TiO_2-1.5, CuO-TiO_2-4 and CuO-TiO_2-8 had bandgap values of 3.36, 3.33, 3.31, 3.27, and 3.25eV, respectively, indicating that the band gap narrows with increasing CuO concentration. CuO supplied more electro-active on the surface of TiO_2 nanocomposites with greater conductivity, which can function as a catalyst in absorption and electrochemical processes, according to electrochemical tests. Photodegradation tests indicated that 100 mg/l of BBF was completely degraded in the presence of CuO/TiO_2 nanocomposites after 60 and 50 min of UV and visible-light irradiation, respectively. These findings suggest that the CuO-TiO_2 nanocomposites can be used to degrade BBF with great efficiency when exposed to visible and UV-light irradiation.

Keywords: Photocatalytic degradation; Brilliant Blue FCF; CuO–TiO2 nanocomposite; UV–Vis absorbance; Cyclic voltammetry

1. INTRODUCTION

Photocatalytic degradation of organic and inorganic contaminants utilizing semiconductor metal oxides shows to have been a highly prominent issue in recent years [1, 2]. Dyes represent a key class of aquatic contaminants, which will have beginning to be a substantial cause of environmental pollution [3, 4]. According to the Food and Drug Administration, dye use has risen significantly between 1955 and 2009 [5, 6]. BBF (Bright Blue FCF) is really a food dye that is usually used in ice cream, dessert powders, baked goods, cereals, drinks, and blue raspberry-flavored products, a variety

of dairy products [7-9]. Human and animal health impacts of BBF have been widely recorded, including gastrointestinal cancers, neurological problems, and severe allergies [10, 11]. Since BBF's molecular structure contains three sulfonic acid groups, it is extremely soluble (200 g/L) [12, 13]. Advanced oxidation methods are promising technologies that use reactive radicals like the hydroxyl radical as a starting place. For the degradation of organic pollutants, the photocatalysis technique is recognized as a green approach [14, 15]. A semiconductor is activated via light-irradiation, and electrons migrate from the valence-bond to the conduction-bond while a hole remains in the valance bond, resulting in the generation of free radicals [16, 17].

Because of its appealing properties such as low cost, non-toxic, good safety, high chemical stability, and strong photo-oxidation potential, TiO_2 has been selected as an appropriate catalyst among semiconductors [18, 19]. TiO_2 has been used as a catalyst for prospective applications such as antibacterial agents, hydrogen generation, self-cleaning surfaces, dye sensitive solar cells, and photocatalytic degradation of dyes because of these capabilities [20-22].

To decrease recombination, the researchers placed the non-metallic semiconductor SiC on the TiO_2 surface [23, 24]. Non-metals, like N and C atoms, electron acceptors, and transition metals, have also been added to TiO_2 to improve solar light-absorbing [25-27]. CuO as a p-type semiconductor has proved to be an effective co-catalyst in photocatalytic water-splitting and also absorbed visible-light region, making it a suitable choice among metal oxides [28, 29].

In this work, CuO-TiO_2 was produced by a simple deposition approach wherein the CuO precursor was applied to TiO_2 slurry and placed in a photoreactor for 12 hours. SEM, XRD, CV, and UV-Vis spectroscopy were used to determine the significant difference between TiO_2 and CuO/TiO_2 nanocomposites. The CuO-TiO_2 nanocomposits were then considered for their performance in BBF degradation with a photodegradation experiment under a photoreactor.

2. MATERIALS AND METHODS

Synthesis of CuO-TiO_2 nanocomposites was done by the photo-assisted deposition technique. In the first step, TiO_2 slurry was made by dissolving 2 grams of TiO_2 powders into 150 mL of distilled water and addition of the nitric acid (96%) to reduce the slurry pH to 3 prior sonicating for 35 minutes. In the second step, $CuCl_2.2H_2O$ was dissolved into 100mL of distilled water with changing mass variations for every sample (0wt%, 0.5wt%, 1.5wt%, 4wt% and 8wt%) and then mixed the solution into TiO_2 slurry, mixing it for 40 minutes before adding 50 mL of pure methanol (96%) to the slurry which is indicated as TiO_2, CuO-TiO_2-0.5, CuO-TiO_2-1.5, CuO-TiO_2-4 and CuO-TiO_2-8, respectively. The slurry is then placed in the photoreactor, where it will be continually irradiated and churned for 5 hours. The slurry is then rinsed until the pH reaches 5 before being separated using a 4000rpm centrifuge for 20 minutes. Finally, the product was kept at 200°C for one hour before being calcined at 300°C.

All photocatalysis tests were carried out in a quartz cylinder reactor with a diameter of 8 cm and a height of 20 cm. The BBF solution was put into the reactor at a volume of 300 mL. KOH and $H2SO_4$ (0.1 M) were used to adjust the pH value of the solution. The solution was mixed using a

mechanical stirrer. The solution was held at 24°C for the duration of the experiment. Two low-pressure lamps (6W) were employed as the UV source in light irradiation, and they were set 2 cm apart on opposite sides of the reactor. Before beginning the photodegradation, the UV lamps were warmed up for 15 minutes. A UV-Vis spectrometer was used to record the BBF's absorption spectra. Monitoring variations in the absorption peaks at 550 nm was used to measure the BBF concentration.

The electrochemical analysis was carried out on an AUTO LAB electrochemical workstation utilizing a traditional three-electrode electrochemical cell with Ag/AgCl as a reference, Pt as a counter, and the produced CuO-TiO_2 nanocomposites on glassy carbon electrodes as working electrodes. In phosphate buffer solutions including 5mM $[Fe(CN)6]^{3-/4-}$, CV measurements were performed. The surface morphology of CuO-TiO_2 nanocomposites was studied using scanning electron microscopy (SEM). The samples' X-ray diffraction (XRD) measurements were performed using a Shimadzu, Japan, D/max 2550Pc automated diffractometer of polycrystalline (CuKα radiation) that worked at 40keV and 100mA at 0.02°/s scanning rate.

3. RESULTS AND DISCUSSION

Figure 1 indicates the SEM images of TiO_2 and CuO-TiO_2-4 nanocomposites which indicate the closely uniform morphology of both samples. Because charge carriers have little effect on the particle size and aggregate of every nanocomposite specimen, the surface area of the CuO-TiO_2 must not change considerably. In particular, it can be deduced that the larger amount of CuO precursors added to the nanocomposites, the further CuO is deposited in TiO_2, resulting in a slight reduction in the nanocomposite's surface area [30].

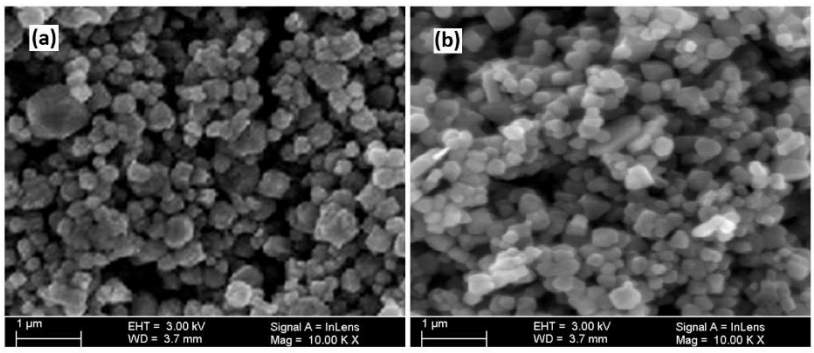

Figure 1. SEM images of (a) TiO2 and (b) CuO-TiO_2-4 nanocomposites

Figure 2 shows the XRD patterns of the as-synthesized samples. The powder materials' peaks are linked to their corresponding crystal planes. The anatase TiO_2 can be accurately ascribed to all diffraction peaks since they are well dunned (JCPDS-21-1272). The photoactivity of anatase TiO_2 nanoparticles was previously known to be high, making them useful for water treatment and

purification [31]. The XRD pattern revealed no distinctive peaks associated with other crystalline forms, suggesting that the product is anatase phase-pure. As shown in Fig. 2, the primary structure of TiO2 is anatase and rutile, with the CuO peak appearing at a loading of 8wt% at 2Θ about 36° [32].

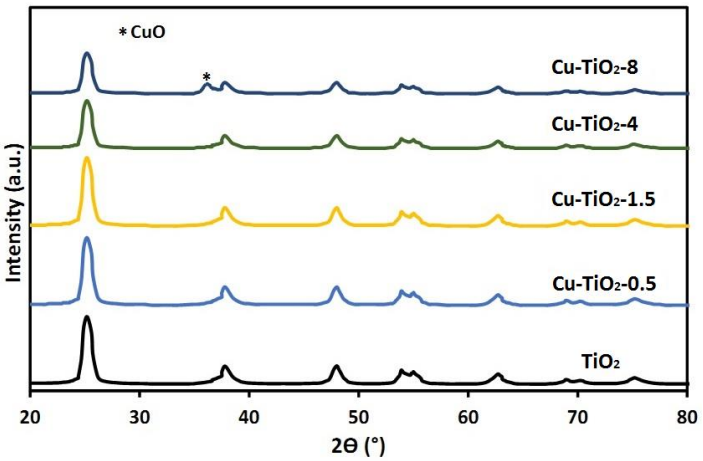

Figure 2. XRD patterns of the as-synthesized samples

Figure 3a shows the UV-visible absorption spectra of CuO-TiO_2nanocomposits with different CuO content at wavelengths ranging from 300 to 900 nm. Because of electrical transitions from the valence band to the conduction band in TiO_2, the absorption spectra show an absorption edge of about 330 nm [33]. When the absorption spectra of TiO_2 and CuO-TiO_2 nanoconposites are compared, the redshift of the absorption edge may be attributed to the decreasing band gap value of CuO-TiO_2 due to CuO's lower Fermi level than TiO_2 [34]. Furthermore, when the amount of CuO in the TiO_2 matrix grows, the redshift rises, which is consistent with other studies [35, 36]. Additionally, increasing the CuO concentration in TiO_2 increases the absorption value, which could be attributed to additional photon absorption sites.

Figure 3b displays the Tauc plots of nanocomposites for determining their optical bandgap (Eg) using the UV-vis absorption spectrum measured and the Tauc equation as follows [37]:

$$(\alpha h\nu)^2=A(h\nu-E_g) \quad (1)$$

Where α shows absorption coefficient, A represents constant, and hν indicates the photon energy. Extrapolating the linear portion of the curve toward the x-axis gives the Eg values. From the Tauc curves in Figure 3b, the Eg values are found TiO_2, CuO-TiO_2-0.5, CuO-TiO_2-1.5, CuO-TiO_2-4 and CuO-TiO_2-8 nanocomposites are found at 3.36, 3.33, 3.31, 3.27, and 3.25eV, respectively. As a result, as the concentration of CuO increases, the Eg values of CuO-TiO_2 nanocomposites decrease. CuO may be incorporated into the TiO_2 structure, resulting in orbitals with intermediate energy levels and electronic interaction between Cu orbital states and O 2p and Ti 3d bands in TiO_2. CuO-TiO_2 nanocomposites with high electronic coupling might generate strong bonds between CuO atoms and

TiO_2 oxygen [38]. CuO-TiO2 nanocomposites have lower Eg values, making them better choices for photocatalytic activity in visible light.

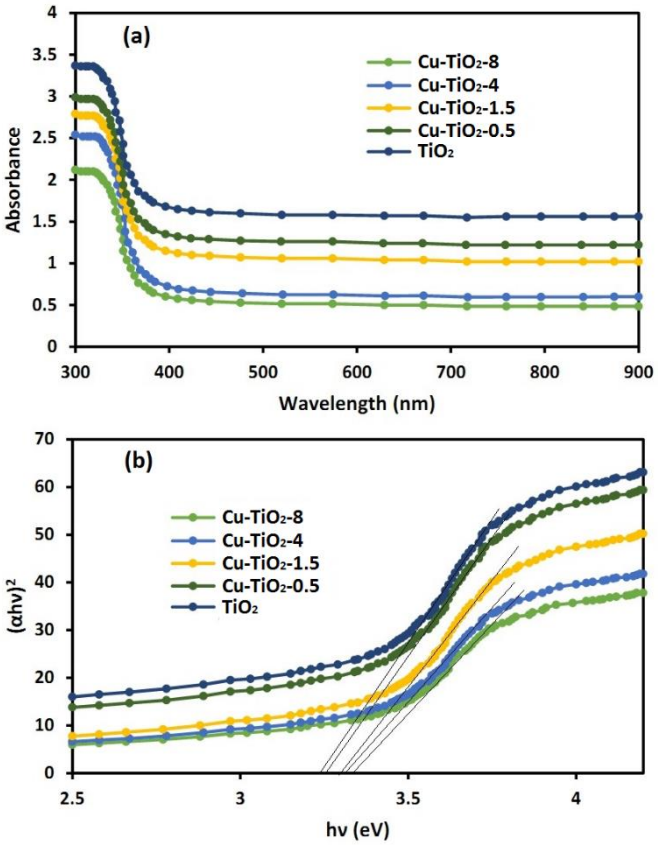

Figure 3. (a) UV-visible absorption spectrum and (b) Tauc plots of TiO_2, CuO-TiO_2-0.5, CuO-TiO_2-1.5, CuO-TiO_2-4 and CuO-TiO_2-8.

Figure 4 shows the CVs of CuO-TiO_2 nanocomposites with various CuO contents in 0.1M PBS (pH 7) with 5mM $[Fe(CN)_6]^{3-/4-}$ as redox-active material at 20 mV/s scan rate. As shown, the cathodic and anodic peak currents are 0.03 and 0.08V for CuO-TiO_2 nanocomposites, respectively. Because conductivity improves with increasing CuO content in TiO2, the current of redox peaks rise, resulting in greater electron transport and charge separation [39, 40]. The decreased charge-transfer resistance can significantly improve the interfacial charge-transfer procedure and contribute more to increased photocatalytic activity by facilitating charge transfer. As a result, as compared to pure TiO_2, the CuO-TiO_2 nanocomposites may have higher photocatalytic activity.

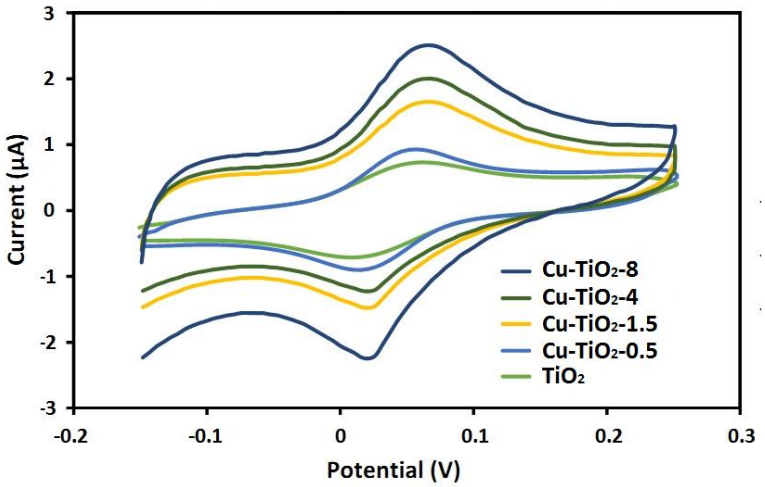

Figure 4. CVs of CuO-TiO_2 nanocomposites with various CuO contents in 0.1M PBS (pH 7) with 5mM $[Fe(CN)_6]^{3-/4-}$ as redox-active material at 20 mV/s scan rate

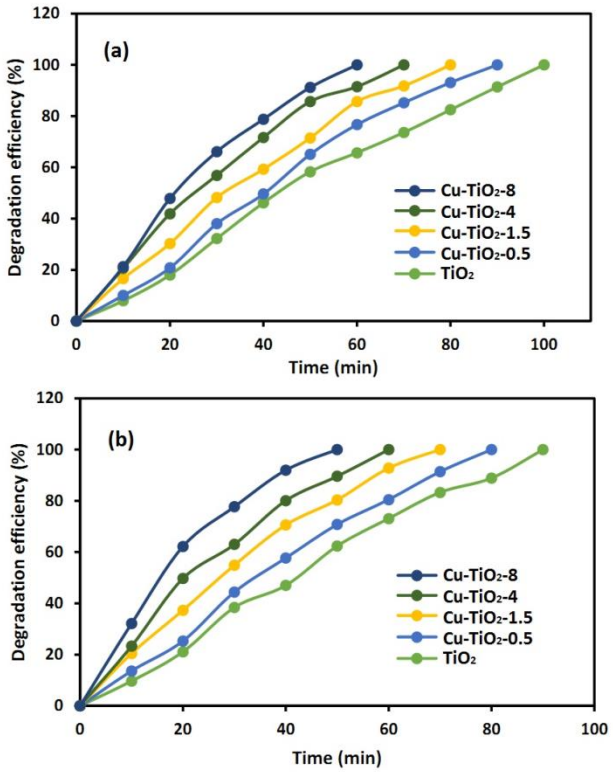

Figure 5. The photocatalytic degradation of 100 mgl^{-1} BBF in solution containing KOH and H_2SO_4 (0.1 M)by CuO-TiO_2 nanocomposites with various CuO contents under (a) UV-light and (b) visible-light irradiationsin at room temperature.

In room temperature visible and UV-light irradiations, the photocatalytic degradation of 100 mgl^{-1} BBFin solution containing KOH and H_2SO_4 (0.1 M) by CuO-TiO_2 nanocomposites with various CuO contents were examined. CuO-TiO_2 nanocomposites have a greater degradation efficiency than pure TiO_2, as shown in figure 5a. After 60 minutes of UV irradiation, the CuO-TiO_2-8 sample had a maximum degradation efficiency of 100%. Figure 5b indicates that increasing CuO content in

nanocomposites increases sample degradation efficiency under visible light irradiation. After 50 minutes of visible irradiation, the CuO-TiO_2-8 nanocomposites were completely degraded. The results indicate that CuO-TiO_2-8 sample has higher photocatalytic activity ~37% and 41% compared to that of pure TiO_2 under UV and visible-light irradiations, respectively. These results show that CuO can enhance the photocatalytic activity of BBF degradation under UV and visible-light irradiations. CuO has a lower Fermi level than TiO2, meaning that it serves as an accumulation center for photo-induced electrons in TiO2 [41]. For CuO-TiO_2-8 specimen, the number of CuO is optimal and the photo-induced electrons remarkably transfer to the CuO. Because photo-generated electrons and holes may be held by adsorbed oxygen to create reactive species superoxide, these accumulation sites can operate as routes for electron separation, lowering the recombination rate of photo-generated holes and electrons [42, 43]. Furthermore, these electrons may react with Ti^{4+} onto a photo-catalyst surface, forming Ti^{3+} reactive sites.

Table 1. Comparison of the obtained results for degradation efficiencies of BBF in CuO-TiO_2 nanocomposites with other reported photocatalysts

Material	**BBF content (mg/l)**	**Light source**	**Degradation time (min)**	**Degradation efficiency (%)**	**Ref.**
CuO-TiO_2	100.00	UV visible	60 50	100 100	This work
Persulfate/zero valent iron	20.00	visible	30	98.9	[44]
Ag-doped ZnO	70.00	UV visible	70 76	49.8 69	[45]
Ag_2O-decorated ZnO	100.00	visible	30	94	[46]
Tungsten doped TiO_2	100.00	sunlight	180	93.25	[47]
TiO_2	20.00	visible	200	88	[48]

In Table 1, the findings of this study was compared to those of other photocatalysts for BBF degradation efficiency. The comparison reveals that CuO-TiO_2 nanocomposites have high photocatalytic activity for the degradation of BBF under visible-light irradiation, which can be ascribed to the synergistic effect of porous structure, which helps facilitate electron-transfer inside the interface between CuO and TiO_2, as well as oxygen vacancies and plentiful anatase, which can enhance charge separation in CuO-TiO_2 nanocomposites [49].

4. CONCLUSIONS

This research focused on a simple deposition method for synthesizing CuO/TiO_2 nanocomposites and their application as photocatalysts for the photodegradation of Bright Blue FCF (BBF) under visible and UV-light irradiations. The prepared nanocomposites and their components

were studied in terms of structural, morphological, electrochemical, optical, and photocatalytic degradation properties. When UV–Vis absorbance spectra were used to characterize photocatalysts, it was revealed that the bandgap reduced as the CuO concentration increased. TiO_2, CuO-TiO_2-0.5, CuO-TiO_2-1.5, CuO-TiO_2-4 and CuO-TiO_2-8 had bandgap values of 3.36, 3.33, 3.31, 3.27, and 3.25eV, respectively, indicating that the band gap narrows with increasing CuO concentration. CuO supplied more electro-active on the surface of TiO_2 nanocomposites with greater conductivity, which can function as a catalyst in absorption and electrochemical processes, according to electrochemical tests. Photodegradation tests revealed that 100 mg/l of BBF was completely degraded in the presence of CuO/TiO_2 nanocomposites after 60 and 50 min of UV and visible-light irradiation, respectively. These findings suggest that the CuO-TiO_2 nanocomposites can be used to degrade BBF with great efficiency when exposed to visible and UV-light irradiation.

References

1. M. Antoniadou, P.P. Falara and V. Likodimos, *Current Opinion in Green and Sustainable Chemistry*, 16 (2021) 100470.
2. C. Chen, X. Wang, Y. Wang, D. Yang, F. Yao, W. Zhang, B. Wang, G.A. Sewvandi, D. Yang and D. Hu, *Advanced Functional Materials*, 30 (2020) 2005141.
3. T. Rasheed, S. Shafi, M. Bilal, T. Hussain, F. Sher and K. Rizwan, *Journal of Molecular Liquids*, 41 (2020) 113960.
4. H. Zhang, W. Guan, L. Zhang, X. Guan and S. Wang, *ACS omega*, 5 (2020) 18007.
5. M.S.A. Reza, M.M. Hasan, M. Kamruzzaman, M.I. Hossain, M.A. Zubair, L. Bari, M.Z. Abedin, M.A. Reza, K.M. Khalid-Bin-Ferdaus and K.M.F. Haque, *Food science & nutrition*, 7 (2019) 667.
6. M. Sun, L. Yan, L. Zhang, L. Song, J. Guo and H. Zhang, *Process biochemistry*, 78 (2019) 108.
7. M.A. Zazouli, F. Ghanbari, M. Yousefi and S. Madihi-Bidgoli, *Journal of environmental chemical engineering*, 5 (2017) 2459.
8. J. Hu, H. Zhang, L. Liu, X. Zhu, C. Zhao and Q. Pan, *IEEE Transactions on Robotics*, 36 (2020) 1805.
9. Z. Wang, Z. Huang, J.T. Brosnahan, S. Zhang, Y. Guo, Y. Guo, L. Wang, Y. Wang and W. Zhan, *Environmental science & technology*, 53 (2019) 5349.
10. X. Shan, Y. Pan, X. Chen, W. Wang and Z. Chen, *Analytical Sciences*, 19 (2019) 18P572.
11. X. Yang, Q. Li, E. Lu, Z. Wang, X. Gong, Z. Yu, Y. Guo, L. Wang and W. Zhan, *Nature communications*, 10 (2019) 1611.
12. I.A. Rodrigues, J.C. Villalba, M.J. Santos, F.L. Melquiades and F.J. Anaissi, *Clay Minerals*, 55 (2020) 12.
13. K. Zhang, Q. Huo, Y.-Y. Zhou, H.-H. Wang, G.-P. Li, Y.-W. Wang and Y.-Y. Wang, *ACS applied materials & interfaces*, 11 (2019) 17368.
14. M. Yadav, S. Garg, A. Chandra and K. Hernadi, *Ceramics International*, 45 (2019) 17715.
15. K. Zhang, Z. Yang, X. Mao, X.-L. Chen, H.-H. Li and Y.-Y. Wang, *ACS applied materials & interfaces*, 12 (2020) 55316.
16. J. Sun, C.-H. Shen, J. Guo, H. Guo, Y.-F. Yin, X.-J. Xu, Z.-H. Fei, Z.-T. Liu and X.-J. Wen, *Journal of Colloid and Interface Science*, 588 (2021) 19.
17. X.-J. Peng, H.-P. He, Q. Liu, K. She, B.-Q. Zhang, H.-S. Wang, H.-T. Tang and Y.-M. Pan, *Science China Chemistry*, 64 (2021) 753.

18. M. Miyake, A. Takahashi and T. Hirato, *International Journal of Electrochemical Science*, 12 (2017) 2344.
19. Q. Wang, S. Sun, X. Zhang, H. Liu, B. Sun and S. Guo, *Bioresource Technology*, 332 (2021) 125120.
20. N.T. Padmanabhan and H. John, *Journal of environmental chemical engineering*, 26 (2020) 104211.
21. L. Zhang, M. Zhang, S. You, D. Ma, J. Zhao and Z. Chen, *Science of The Total Environment*, 780 (2021) 146505.
22. J.-Z. Cheng, Z.-R. Tan, Y.-Q. Xing, Z.-Q. Shen, Y.-J. Zhang, L.-L. Liu, K. Yang, L. Chen and S.-Y. Liu, *Journal of Materials Chemistry A*, 9 (2021) 5787.
23. U. Baig, M. Gondal, M. Dastageer, A. Khalil and S. Zubair, *Journal of Photochemistry and Photobiology B: Biology*, 187 (2018) 113.
24. X. Li, T. Shi, B. Li, X. Chen, C. Zhang, Z. Guo and Q. Zhang, *Materials & Design*, 183 (2019) 108152.
25. S.B. Patil, P.S. Basavarajappa, N. Ganganagappa, M. Jyothi, A. Raghu and K.R. Reddy, *International Journal of Hydrogen Energy*, 44 (2019) 13022.
26. J.-B. Liu, M. Ren, X. Lai and G. Qiu, *Chemical Communications*, 57 (2021) 4259.
27. Y. Duan, Y. Liu, Z. Chen, D. Liu, E. Yu, X. Zhang, H. Fu, J. Fu, J. Zhang and H. Du, *Green Chemistry*, 22 (2020) 44.
28. W. Li, S.-a. He, Z.-y. Su, W. Xu and X.-c. Wang, *Applied Surface Science*, 470 (2019) 707.
29. Y. Liu, X. Lv and Z. Tang, *Personality and Individual Differences*, 180 (2021) 110972.
30. A. Manivel, S. Naveenraj, P.S. Sathish Kumar and S. Anandan, *Science of Advanced Materials*, 2 (2010) 51.
31. K.E. Greenstein, M.R. Nagorzanski, B. Kelsay, E.M. Verdugo, N.V. Myung, G.F. Parkin and D.M. Cwiertny, *Environmental Science: Nano*, 8 (2021) 711.
32. D.M. Tobaldi, C. Espro, S.G. Leonardi, L. Lajaunie, M.P. Seabra, J.J. Calvino, S. Marini, J.A. Labrincha and G. Neri, *Journal of Materials Chemistry C*, 8 (2020) 9529.
33. M. Navarrete, S. Cipagauta-Díaz and R. Gómez, *Journal of Chemical Technology & Biotechnology*, 94 (2019) 3457.
34. R. Nekooie, T. Shamspur and A. Mostafavi, *Journal of Photochemistry and Photobiology A: Chemistry*, 407 (2021) 113038.
35. F. Hayati, M.R. Khodabakhshi, A.A. Isari, S. Moradi and B. Kakavandi, *Journal of Water Process Engineering*, 38 (2020) 101693.
36. Y. Yang, H. Chen, X. Zou, X.-L. Shi, W.-D. Liu, L. Feng, G. Suo, X. Hou, X. Ye and L. Zhang, *ACS applied materials & interfaces*, 12 (2020) 24845.
37. L. Xiaojiao, Y. Junchuan, Z. Jiawei, L. Ming, Y. Peizhi and H. Zhihua, *International Journal of Electrochemical Science*, 11 (2016) 10827.
38. Q. Shi, Z. Qin, C. Yu, A. Waheed, H. Xu, Y. Gao, H. Abroshan and G. Li, *Nano Research*, 29 (2020) 1.
39. Z. Li, Y. Qu, G. He, M. Humayun, S. Chen and L. Jing, *Applied Surface Science*, 351 (2015) 681.
40. Z. Chen, H. Zhang, X. He, G. Fan, X. Li, Z. He, G. Wang and L. Zhang, *BioResources*, 16 (2021) 2644.
41. S. Xu, J. Ng, X. Zhang, H. Bai and D.D. Sun, *International Journal of Hydrogen Energy*, 35 (2010) 5254.
42. M. Pandiri, R. Velchuri, R. Gundeboina and V. Muga, *Journal of Photochemistry and Photobiology A: Chemistry*, 360 (2018) 231.
43. S. Zhang, S. Zhao, S. Huang, B. Hu, M. Wang, Z. Zhang, L. He and M. Du, *Chemical Engineering Journal*, 420 (2021) 130516.

44. M. Yousefi, F. Ghanbari, M.A. Zazouli and S. Madihi-Bidgoli, *Desalin. Water Treat*, 70 (2017) 364.
45. T. Parvin, N. Keerthiraj, I.A. Ibrahim, S. Phanichphant and K. Byrappa, *International Journal of Photoenergy*, 2012 (2012) 1.
46. R. Lamba, A. Umar, S. Mehta and S.K. Kansal, *Separation and Purification Technology*, 183 (2017) 341.
47. B. Shahmoradi, A. Maleki and K. Byrappa, *Catalysis Science & Technology*, 1 (2011) 1216.
48. G.S. Jeong and S.I. Choe, *Journal of Environmental Science International*, 13 (2004) 599.
49. D. Nagy, C. Chao, B. Marzec, F. Nudelman, M.-C. Ferrari and X. Fan, *Journal of environmental management*, 260 (2020) 110175.